Geophysical Research Letters

RESEARCH LETTER
10.1029/2022GL098102

Snow Albedo Feedbacks Enhance Snow Impurity-Induced Radiative Forcing in the Sierra Nevada

Huilin Huang[1], Yun Qian[1], Cenlin He[2], Edward H. Bair[3], and Karl Rittger[4]

[1]Pacific Northwest National Laboratory, Atmospheric Sciences and Global Change Division, Richland, WA, USA, [2]Research Applications Laboratory, National Center for Atmospheric Research, Boulder, CO, USA, [3]Earth Research Institute, University of California, Santa Barbara, CA, USA, [4]Institute for Arctic and Alpine Research, University of Colorado Boulder, Boulder, CO, USA

Key Points:

- Light-absorbing particles decrease snow albedo by up to 0.045 during April–July, producing radiative forcing of up to 22 W m^{-2}
- Impurity effects are amplified by a factor of 2–3 due to snow albedo feedbacks associated with snow aging and snow cover change
- Impurity effects decrease snow water equivalent by 20 mm in June and reduce root zone soil water content by 20% in bighorn sheep habitat

Supporting Information:

Supporting Information may be found in the online version of this article.

Correspondence to:

H. Huang and Y. Qian,
Huilin.huang@pnnl.gov;
Yun.Qian@pnnl.gov

Citation:

Huang, H., Qian, Y., He, C., Bair, E. H., & Rittger, K. (2022). Snow albedo feedbacks enhance snow impurity-induced radiative forcing in the Sierra Nevada. *Geophysical Research Letters*, *49*, e2022GL098102. https://doi.org/10.1029/2022GL098102

Received 29 JAN 2022
Accepted 15 MAY 2022

Author Contributions:

Conceptualization: Yun Qian
Methodology: Cenlin He
Supervision: Yun Qian
Validation: Edward H. Bair, Karl Rittger
Writing – review & editing: Yun Qian, Cenlin He, Edward H. Bair, Karl Rittger

Abstract This study employs a fully coupled meteorology-chemistry-snow model to investigate the impacts of light-absorbing particles (LAPs) on snow darkening in the Sierra Nevada. After comprehensive evaluation with spatially and temporally complete satellite retrievals, the model shows that LAPs in snow reduce snow albedo by 0.013 (0–0.045) in the Sierra Nevada during the ablation season (April-July), producing a midday mean radiative forcing of 4.5 W m^{-2} which increases to 15–22 W m^{-2} in July. LAPs in snow accelerate snow aging processes and reduce snow cover fraction, which doubles the albedo change and radiative forcing caused by LAPs. The impurity-induced snow darkening effects decrease snow water equivalent and snow depth by 20 and 70 mm in June in the Sierra Nevada bighorn sheep habitat. The earlier snowmelt reduces root-zone soil water content by 20%, deteriorating the forage productivity and playing a negative role in the survival of bighorn sheep.

Plain Language Summary Snowpacks in the Sierra Nevada receive large amounts of light-absorbing particles [LAPs, mainly dust and black carbon (BC)], which decrease snow albedo, induce additional radiative forcing, alter the balance between snowmelt water supply and water demand, and influence the survival and resource selection of the Sierra Nevada bighorn sheep. However, quantifications of LAP-induced snow darkening effects were rare in the Sierra Nevada and showed large spatial variability. Employing a fully coupled meteorology-chemistry-snow model, our study shows that snow albedo is reduced by up to 0.045 during April–July, which produces a radiative forcing of up to 22 W m^{-2}. The darkened snow absorbs more sunlight, which decreases the snow water equivalent by 20 mm and shifts the melting season earlier. As a result, the root-zone soil water content and forage productivity are reduced in early summer, which tends to deteriorate bighorn sheep nutrition levels and is harmful to their survival.

1. Introduction

The mountain snow located in the Sierra Nevada (SN) receives precipitation during winter and gradually releases melting water through the spring and dry summer, acting as low-cost water storage. The snowmelt runoff is captured by reservoirs and released to the downstream community, contributing to 60% of the state's consumptive water supply (Avanzi, 2018). The snowpack also plays a vital role in the survival of the Sierra Nevada bighorn sheep, an endangered subspecies of bighorn sheep living in the mid-high elevations of the SN. During winter, aboveground snow impedes the travel of bighorn sheep and reduces the forage availability (Conner et al., 2018), while melting snow supplies soil water for plant growth and influences the nutrition level of bighorn sheep in the following spring and summer (Monteith et al., 2014; Stephenson et al., 2020).

The general balance between snowmelt water supply and water demand in the SN is challenged due to decreased peak snow volume and earlier snowmelt in a changing climate (Huning & AghaKouchak, 2018; Kapnick & Hall, 2010; Wanders et al., 2017). Light-absorbing particles (LAPs) in snow, mainly dust and black carbon (BC), enhance melting by decreasing surface albedo in the visible and near-infrared, referred to as the "instantaneous snow darkening effects" (Hadley & Kirchstetter, 2012; Hadley et al., 2010; Qian, Wang, et al., 2014; Qian, Yasunari, et al., 2014; Skiles et al., 2018; Warren & Wiscombe, 1980). The darkened snow absorbs more sunlight, accelerating snow aging, increasing snow grain sizes, and exposing more dark surfaces, known as the "snow albedo feedback" which further reduces surface albedo (Myhre et al., 2013). The snow darkening effects have large spatial variability and are influenced by the LAP emissions, transport, and post-depositional processes

(Kang et al., 2020). Over the Himalaya and the Arctic, LAPs in snow are found to have comparable radiative forcing (RF) to greenhouse gases (Flanner et al., 2007). Snowpacks in the SN also receive large amounts of LAPs from local and remote sources. The ambient dust in the atmosphere is produced from sources such as the dry Owens Lake and the Sonoran Desert (Duniway et al., 2019; Reheis, 1997; Reheis & Kihl, 1995) or transported from as far away as the Sahara and Asia (Creamean et al., 2013). Meanwhile, BC emitted from coastal metropolitan regions, forest fire, or originating from Asia can also be carried to the SN by prevailing westerlies (Hadley et al., 2010; Huang et al., 2020).

While impurity effects have been extensively observed and modeled in the Himalaya and the Rocky Mountains (C. Wu et al., 2018; He et al., 2018; Niu et al., 2018; Oaida et al., 2015; Painter et al., 2007, 2010; Qian et al., 2011; Rahimi et al., 2020; Sarangi et al., 2019, 2020; Skiles & Painter, 2017, 2018), their quantification in the SN is lacking. Observational studies have focused on specific areas and reported a wide range of RF induced by impurities in snow. Sterle et al. (2013) reported a BC concentration of 20–429 ng g^{-1} and a dust concentration of 1–44 μg g^{-1} on the snow surface of Mammoth Mountain, which combined contributed to 20–40 W m^{-2} RF during the 2009 ablation season. Airborne observations over Kaweah/Kings river basins showed that LAPs reduced albedo from 0.70 to 0.55 and caused an RF of 0–150 W m^{-2} (Seidel et al., 2016). The LAP effects show large spatial variability; it is therefore difficult to apply the conclusions to other basins or make inferences at the regional scale.

The Weather Research and Forecasting (WRF) model coupled with online chemistry (WRF-Chem) has been widely used to assess the interactions between aerosols and snow at the regional scale. As a widely used regional climate model, WRF has been shown to capture fine-scale precipitation and snow features (Chen, Duan, et al., 2019; Chen, Leung, et al., 2019). An early WRF-Chem study found that BC reduced albedo by 0.01–0.03 and caused an RF of 1–3 W m^{-2} in the SN (Qian et al., 2009). The result was generally confirmed by Hadley et al. (2010), which used observed BC concentrations in the NCAR CCM3_CRM radiation model to calculate RF induced by BC in snow. Neither study considered the effects of dust in snow, which was observed to play a dominant role in the eastern SN. A recent modeling study by L. Wu et al. (2018) moved further to assess the aerosol–snow interactions due to both BC and dust and compared it with other pathways of aerosol effects: aerosol–radiation interactions and aerosol–cloud interactions. Yet the simulated albedo change has not been thoroughly evaluated due to a lack of observations in the SN. The recently developed satellite products, such as the MODIS Snow-Covered Area and Grain size algorithm (MODSCAG; Painter et al., 2009) and Snow Property Inversion from Remote Sensing (SPIReS; Bair et al., 2020) retrieve snow properties on the regional scale with complete temporal coverage. They provide instantaneous snow darkening effects for the time satellite overpasses the target pixels, which is especially important in regions with rare site measurements. In addition, the instantaneous darkening effects and snow albedo feedbacks associated with snow aging and snow cover change are two important processes influencing LAP's darkening effects. Their relative contributions have not been well understood in previous studies. Furthermore, there is a lack of process-level analyses on how snow darkening effects evolve with LAPs depositions, precipitation, snow aging, and meltwater runoff across the SN, which would facilitate a more realistic prediction of snow darkening effects in a changing world.

The objective of this study is: (a) to evaluate the WRF-Chem representation of snow properties and snow darkening effects against satellite retrievals and elucidate model uncertainties in the SN; (b) to separate and quantify instantaneous darkening effects and the snow albedo feedbacks associated with snow aging and snow cover change; (c) to comprehensively analyze the snow darkening effects caused by LAPs' deposition, precipitation, snow aging, and meltwater scavenging processes.

2. Model and Method

2.1. Model and Input Data

We used the state-of-the-art WRF-Chem version 3.9 coupled with the Community Land Model (CLM4) land surface scheme, and the Snow, Ice, Aerosol, and Radiation model (SNICAR) to study snow evolution in the SN. This coupled model is referred to as WCCS hereafter. In WCCS, we chose the Model of Ozone and Related chemical Tracers (MOZART) chemistry module (Emmons et al., 2020) and the Model for Simulating Aerosol Interactions and Chemistry with four bins (MOSAIC 4-bin) aerosol model (Zaveri & Peters, 1999) for comprehensive treatment for gas chemistry and aerosol processes (Table S2 in Supporting Infomation S1). The

SNICAR simulates the snow properties and associated radiative heating rates of multilayer snowpack (Flanner et al., 2009, 2021) and is used within CLM, which provides the number of snow layers and meltwater transport from each layer (Oleson et al., 2010). Following the methodology in Zhao et al. (2014), we coupled the WRF-Chem simulated aerosols with CLM-SNICAR to simulate the aerosol radiative effects in snowpack. Modifications have been made as we used the MOZART in WRF-Chem v3.9 instead of the CBM-Z (carbon bond mechanism) in WRF-Chem v3.5 in Zhao et al. (2014). A detailed description of the coupling strategy is provided in Text S1 of Supporting Information S1.

The meteorological initial and lateral boundary conditions were derived from the ECMWF Reanalysis v5 [ERA5 (Hersbach et al., 2020)] at 0.25° horizontal resolution and 6 hr temporal intervals. Spectral nudging was employed with a timescale of 6 hr above the boundary layer to reduce the drift between ERA5 reanalysis data and WRF's internal tendencies (von Storch et al., 2000). The MYJ (Mellor–Yamada–Janjic) planetary boundary layer scheme (Hong et al., 2006), Morrison 2-moment microphysics scheme (Morrison et al., 2009), Grell-Freitas cumulus scheme (Grell & Freitas, 2014), and RRTMG longwave and shortwave radiation schemes (Iacono et al., 2008) were used in this study.

Anthropogenic emissions provided by the US EPA 2017 National Emissions Inventory (US Environmental Protection Agency, 2021) were updated every hour to account for the diurnal variability. Fire INventory from NCAR version 2.4 (FINNv2.4) provided daily biomass burning emissions for the years 2018 and 2019 (Wiedinmyer et al., 2014). Biogenic emissions were generated using the Model of Emissions of Gases and Aerosols from Nature (MEGAN) (Guenther et al., 2006). Dust emissions were calculated "online" using the GOCART dust scheme (Ginoux et al., 2001), and here, we increased the emission parameter from 1×10^{-9} to 5×10^{-9} kg m^{-5}s^2 C in Equation S1 in Supporting Information S1 to match the measurements of surface dust concentration (Text S2 in Supporting Information S1). The chemical initial and boundary conditions were provided by CAM-Chem (Buchholz et al., 2019).

2.2. Numerical Experiments

The WCCS experiment was configured to cover all of California, Nevada, and part of the surrounding states (126.12–112.86°W, 32.3–43.0°N) with 110 × 120 grid cells at 10 × 10 km^2 horizontal resolution (Figure 1a). We used 35 vertical model layers from the surface to 10 hPa with denser layers at lower altitudes to resolve the planetary boundary layer. The simulation period ranged from 20 September 2018, to 31 August 2019, to allow for the accumulation and ablation of snowpacks in a water year. Only the results after 1 October 2018 were analyzed to minimize the impacts of initial conditions. To quantify the effects of LAPs in snow with and without snow albedo feedbacks, we designed the following two experiments:

1. $WCCS_{aero}$ simulated the direct and indirect effects of aerosols in the atmosphere and the effects of LAPs in snow.
2. $WCCS_{noaero}$ is similar to $WCCS_{aero}$ except that the impurity effects in snow were not included. The deposited LAPs in snow were manually set to 0 in CLM-SNICAR.

$WCCS_{aero}$ calculated the instantaneous snow albedo reduction and RF caused by LAPs in every model timestep by contrasting the dirty and clean snow albedo under current snow cover, which can be used to evaluate the LAPs' instantaneous snow darkening effects. The difference between $WCCS_{aero}$ and $WCCS_{noaero}$ showed the changes of snow albedo and RF due to both instantaneous snow darkening effects and snow albedo feedbacks associated with snow aging and snow cover change. The RF refers to the change in net (down minus up) solar irradiance at the surface caused by the impurity effects (instantaneous darkening effects with/without snow albedo feedbacks).

2.3. Validation Data

The simulated aerosols from 2018 October to 2019 August were compared against PM2.5 observations from U.S. EPA Outdoor Air Quality Data (US Environmental Protection Agency, 2021) and IMPROVE (Interagency Monitoring of Protected Visual Environments, Access date October 2021 [Malm et al., 1994]), and aerosol surface concentration from IMPROVE measurements. We evaluated the simulated snow water equivalent (SWE) with the SNODAS (Snow Data Assimilation System), which assimilated satellite-derived, airborne, and ground-based snow observations into an operational snow accumulation and ablation model (Barrett, 2003), and we evaluated

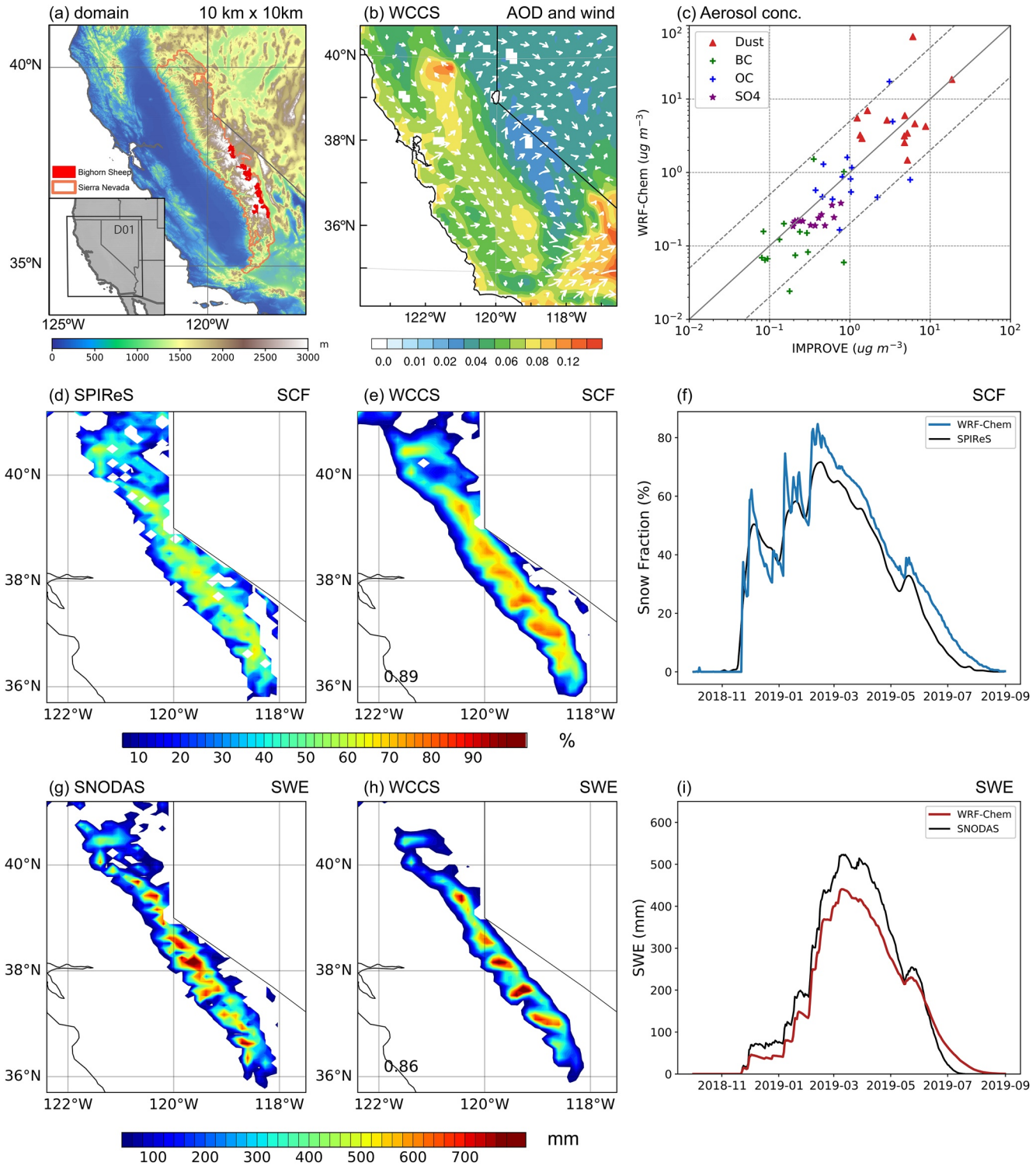

Figure 1. (a) Sierra Nevada region and bighorn sheep habitat, the inserted plot shows $WCCS_{aero}$ simulation domain (D01); (b) modeled AOD with wind vector overlaid; (c) surface concentrations of dust, black carbon (BC), OC, and SO4 in the model compared with IMPROVE observations; (d)–(e) snow cover fraction (SCF) in model and SPIReS; (f) daily SCF in $WCCS_{aero}$ and SPIReS averaged over the Sierra Nevada; (g)–(i) same as (d)–(f) but for snow water equivalent (SWE). Variables in panels (b)–(e) and (g)–(h) are averaged over October 2018 and August 2019.

snow cover fraction (SCF) with SPIReS retrievals (Bair et al., 2020). SPIReS was also used to estimate albedo degradation due to LAPs using the difference between modeled clean and observed (dirty) snow albedo. Both SNODAS and SPIReS have been upscaled to the model resolution before comparing them with the simulation results.

3. Results

3.1. Model Evaluation

Figure 1b shows the spatial distribution of AOD averaged from 2018 October to 2019 August. The AOD maxima in northern California are caused by the emissions during the Camp fire in November 2018, the most destructive and deadliest fire in California history. Additionally, high AOD values are found in the San Joaquin Valley and metropolitan areas such as San Francisco. The urban emissions are transported eastward and are blocked by mountains, producing a minimum AOD on the eastern slope of SN. Meanwhile, high AOD is also shown over southeastern California, due to the dust emissions from the Mojave Desert. The PM2.5 surface concentrations show a similar spatial distribution to AOD (Figure S1 in Supporting Information S1), with slight underestimations compared to EPA and IMPROVE measurements in the Central Valley and overestimations in southern California. The modeled surface aerosol concentrations are generally within a factor of five of the observed concentrations from IMPROVE sites (Figure 1c). After the calibration of the GOCART dust scheme, simulated dust concentration appears unbiased compared to observed dust concentration. Nevertheless, anthropogenic aerosol concentrations (BC, organic carbon, and sulfate) are underestimated compared to the observations, which is a common problem in WRF-Chem simulations in California and might be related to the coarser model resolution, uncertainties in emission inventory, and/or a lack of important chemical processes in the model (Wang et al., 2020; L. Wu et al., 2017; Zhao et al., 2013).

We evaluate SCF and SWE with multiple observations during the reference period. The heights of mountain peaks increase gradually from north to south (Figure 1a), and correspondingly, large SCFs are found in the southern SN (Figures 1d and 1e). Snowpacks in low elevations (in both northern and southern SN) diminish in April, while snowpacks in the northern SN (>1,500 m elevation) melt out in May, and snowpacks at the top of the southeast SN last until early August. Compared to SPIReS, $WCCS_{aero}$ reproduces the spatial distribution of SCFs with a correlation coefficient of 0.89 and appropriately captures the temporal evolution (Figure 1f). $WCCS_{aero}$ overestimates SCF in the southern part of the SN, which probably comes from precipitation biases due to the coarser terrain representation (not shown). $WCCS_{aero}$ underestimates peak SWE compared to SNODAS (Figures 1g–1i), yet the latter is shown to overestimate SWE in multiple years (Bair et al., 2016). For the 2019 water year, we use April–July as the ablation season to assess the LAP effects in snow in the SN.

3.2. Snow Darkening and Radiative Forcing Due To LAP Effects

LAP effects in the snowpack are closely related to the microphysical properties of snowpack, for example, snow grain sizes (SGSs). Annual SGSs from SPIReS range from 54 to 530 μm in the SN, with a regional average of 285 μm (Figure 2a). The regional average SGS in $WCCS_{aero}$ is larger compared to the remotely sensed observations (315 μm) with a smaller spatial variability from 113 to 476 μm (Figure 2b). SGSs are small during winter and rapidly grow in spring because of snow grain metamorphism driven by high temperatures and strong incident irradiance (Flanner & Zender, 2006; Painter et al., 2003, 2013). Larger SGSs are found in the northern SN as warmer temperatures in low elevations facilitate snow aging processes. SGSs at higher elevations (>2,500 m) increase significantly in the late ablation period, producing larger SGSs at the annual time scale in SPIReS (Figure 2a). The model underestimates SGSs growth in the late melting season, therefore producing smaller SGSs at higher elevations as compared to SPIReS (Figure 2b). Retrieved SGSs at lower elevations might be underestimated as these pixels are normally partially covered by snow (SCF <90%) and are interpolated with relatively pure snow pixels (SCF ≥90%) from higher elevations with smaller grain sizes (Bair et al., 2020).

The concentrations of dust and BC on the snow surface range between 4 and 30 μg g^{-1} and 10–40 ng g^{-1} respectively during March-May, with small variations among different elevations (Figure S2 in Supporting Information S1). Both concentrations increase by a factor of 2–4 as snow melts. In June, the BC concentration decreases with elevation while the dust concentration peaks in both low elevations (1,500–2,000 m) and mid elevations (2,500 m). Our simulated LAPs concentration is generally consistent with Hadley et al. (2010) who reported

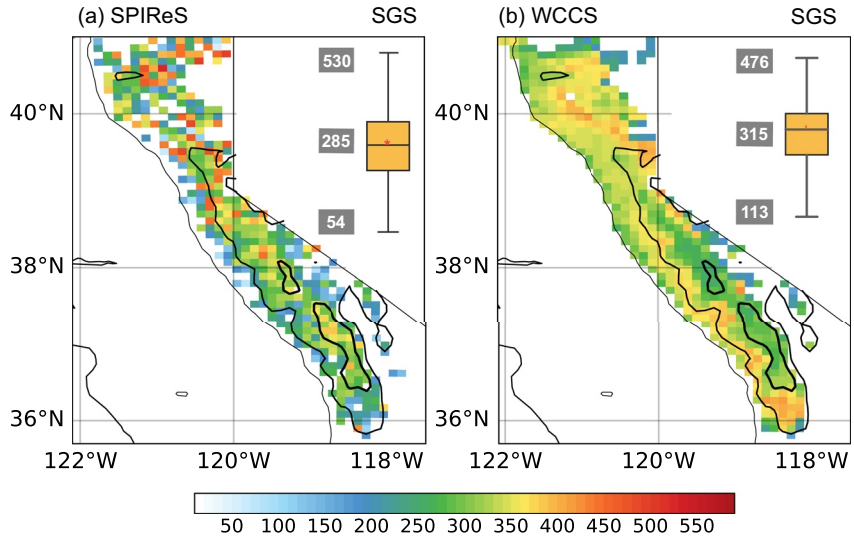

Figure 2. Annual mean snow grain sizes (SGSs) in (a) SPIReS and (b) $WCCS_{aero}$ averaged over 2018 October to 2019 August. The box plots illustrate the distribution of SGSs in SPIReS and WCCS throughout the Sierra Nevada with the mean, maximum and minimum values labeled on the left. The three contours with different thickness represent the elevations of 1,000, 2,000, and 3,000 m.

BC concentrations of 5.3 and 6.9 ng g^{-1} in falling snow during March–April 2006 at two SN locations. At Mammoth Mountain Ski Area, Sterle et al. (2013) found that BC concentration increased from 25 ng g^{-1} during January-April to 135 ng g^{-1} in May 2009 while dust concentration (12 μg g^{-1}) remained relatively stable during the ablation season.

The dust and BC in snow cause snow darkening which accelerates the snow aging process (Lee & Liou, 2012; Qian, Yasunari, et al., 2014). Satellite retrievals show that the LAP-induced snow albedo decrease ($\Delta\alpha$, larger $\Delta\alpha$ represents higher albedo reduction) during April-July can be as large as 0.068, with an average of 0.016 over the SN (Figure 3a). The $\Delta\alpha$ in $WCCS_{aero}$ spans between 0.0 and 0.045, with a spatial average of 0.013 (Figure 3b), slightly lower than the estimate from SPIReS, especially at higher elevations. The estimated $\Delta\alpha$ is larger in $WCCS_{aero}$ than SPIReS at lower elevations, while we note that SPIReS might have underestimated $\Delta\alpha$ as it interpolates pixels at lower elevations with pure snow pixels (larger albedo) from higher elevations. In both the model and remotely sensed observations, the LAP-induced $\Delta\alpha$ first appears at lower elevations with relatively higher temperatures and thinner snowpacks (Figure S3 in Supporting Information S1). The $\Delta\alpha$ in the southern SN higher elevations is small in the early melting season and greatly increases in June and July, corresponding to the later snowmelt there. The model generally captures the spatial distribution of $\Delta\alpha$ at the monthly scale but underestimates $\Delta\alpha$ in June and July. Throughout the SN, we find LAPs in snow cause an RF of 4.5 W m^{-2} (Figure 3c). The largest RF (14.6 W m^{-2}) is found in the southeast SN with higher elevations, despite the lowest AOD there. This is because higher elevations have a later onset of snowmelt and therefore receive higher solar irradiance during the ablation period. The bighorn sheep habitat (Figure 1a red area), with an elevation of 2,840 m on average, is found to have an RF of 12.3 W m^{-2} during the melting season, which can reach 45 W m^{-2} in mid-June.

Figure 3d shows the evolution of $\Delta\alpha$ caused by LAPs in snow at different elevations. The albedo degradation is less than 0.01 during March-April, which has a steep increase to 0.02 in late May. At lower elevations (1–2 km), the snow darkening effect peaks in late June before snowpacks melt out, while it reaches 0.08 in late August at the higher elevations. The corresponding RF on snow remains generally smaller than 5 W m^{-2} before June and rapidly increases to 15–22 W m^{-2} in July. The contribution from dust is larger in the eastern SN adjacent to the desert, while the contribution from BC is larger in the northwestern SN near the anthropogenic emission and fire emission sources (not shown). Here we focus on dust deposition and accumulation in snow, noting that the BC shows similar changes. The dust concentration on the snow surface varies from 10 to 100 μg g^{-1}. During March–May, the deposited dust particles are buried by frequent snowfalls, which add fresh snow with smaller grain sizes to the ground (Figure 3e) and cover surface dust with resulting concentrations at lower levels (Figure 3d). As a result, the LAP-induced $\Delta\alpha$ and RF are small. The abrupt decreases of SGSs after snowfalls were also reported in

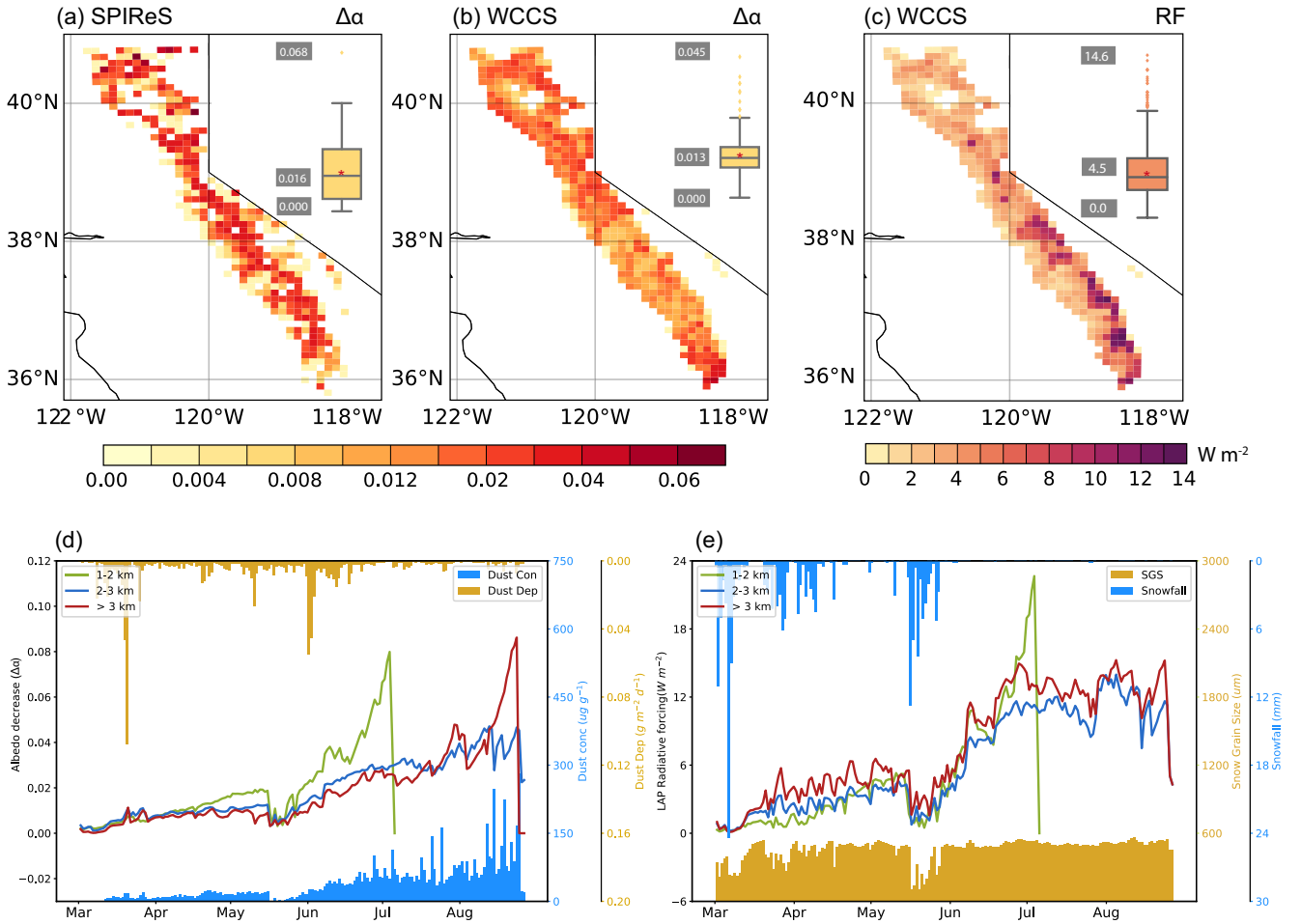

Figure 3. Spatial distribution of snow albedo decrease ($\Delta\alpha$) in (a) SPIReS retrievals (b) $WCCS_{aero}$ and (c) RF in $WCCS_{aero}$ during midday (10:00–14:00 LT) averaged over April–July. The box plots illustrate the distribution of $\Delta\alpha$ (RF) throughout the Sierra Nevada with the mean, maximum and minimum values labeled on the left; (d) March–August albedo decrease ($\Delta\alpha$) during midday (10:00–14:00 LT) at different elevations in $WCCS_{aero}$. The light blue bars show dust concentration on the top snow layer while the yellow bars show dust deposition, averaged over the Sierra Nevada; (e) Simulated RF at different elevations. The yellow bar shows snow grain sizes while the light blue bars show snowfall over the Sierra Nevada.

Seidel et al. (2016) but the magnitude is smaller than our simulation (330–180 μm in observations compared to ~450 to 100 μm in $WCCS_{aero}$). As snowpacks melt, some dust particles are scavenged away in meltwater but most accumulate, especially at the snow surface (Doherty et al., 2010; Flanner et al., 2007), reflected by the increase of dust concentration by a factor of 4 in the late ablation season. The enrichment of dust concentration exacerbates the increase of $\Delta\alpha$ and RF in June and July (Figure 3d).

The underestimation of LAP effects compared to the remotely sensed retrievals can be explained by several aspects. First, $WCCS_{aero}$ underestimates BC surface concentration and might also underestimate BC concentration in snow and BC-induced LAP effects over the west slope of the SN. Furthermore, the radiative effect of LAPs in snow is amplified with increasing SGSs (Warren & Wiscombe, 1980). The underestimated $\Delta\alpha$ at higher elevations in $WCCS_{aero}$ is probably due to insufficient SGSs increases in the late melting season, reflected by the smaller SGSs at the higher elevations compared to SPIReS (Figure 2). Besides, the version of CLM-SNICAR within $WCCS_{aero}$ does not consider the internal mixing of dust, which is shown to enhance $\Delta\alpha$ by 10%–30% for dust relative to the external mixing states (He et al., 2019). Additionally, the structure packing of snow grains is suggested to enhance the LAP-induced albedo reduction (He, Takano, & Liou, 2017) which is not considered in the model. Conversely, grains are assumed spherical in SNICAR-CLM, which is not always a correct approximation (He, Takano, Liou, et al., 2017), yet nonspherical snow grains produce smaller radiative effects compared to spherical grains (Dang et al., 2016) and are thus not a cause of underestimated LAP effects. Moreover, SPIReS

estimates $\Delta\alpha$ based on surface reflectance changes contributed by multiple LAPs [carbon, dust, and algae (Bair et al., 2021)], while our simulation does not consider the effects from brown carbon or snow algae (Kirchstetter et al., 2004; Painter et al., 2001; Thomas & Duval, 1995).

While we use satellite measurements as ground truth, we note that multiple factors may induce the uncertainties in products, including off-nadir viewing effects, geolocation errors, misclassification between clouds and snow, and errors in the atmospheric model retrieving the aerosol optical depth (Bair et al., 2019, 2020; Stillinger et al., 2019). Extensive validations were conducted against site observations across the western US with RMSE values of 4%–6% in broadband snow albedo between SPIReS and site measurements (Bair et al., 2019). Besides, $\Delta\alpha$ from SPIReS is calculated using the difference between observed snow albedo and modeled clean snow albedo; the latter is associated with SGS retrieval, which could also be biased due to the abovementioned uncertainties. In addition, Bair et al. (2020) have made a few assumptions to reduce uncertainties in pixels partially covered by snow: (a) Relatively pure pixels (snow cover fraction >0.90) are used to interpolate SGS to pixels partially covered by snow and therefore produce smaller SGS and (b) Pixels with small SGS (<400 μm) are assumed to be clean. Both assumptions may cause underestimation of LAP-induced $\Delta\alpha$.

3.3. LAP Effect Due To Snow Albedo Feedback

We assess how the snow albedo feedback plays a role in the snow darkening effects by comparing the $WCCS_{aero}$ with $WCCS_{noaero}$. Grid-averaged surface albedo changes are discussed afterward as snow cover is different in both experiments. The regional albedo decrease is 0.008 averaged across the SN, doubling the value (0.004) we found in LAPs' instantaneous snow darkening effects (Figure 3b), due to the additional role of snow albedo feedbacks associated with snow aging and snow cover fraction. The albedo reduction is positively correlated with elevation and reaches 0.04 in the southeast SN (Figure 4a). The simulated albedo change is slightly higher than model estimates from L. Wu et al. (2018). The calibrated larger dust emission may produce a larger albedo degradation. Other factors such as different anthropogenic and fire emissions inventories and lateral boundary conditions could also play a role. The albedo change increases solar radiation absorption by about 8.5 W m^{-2} during the midday, with the largest RF reaching 40 W m^{-2} within the high elevations of southern SN (Figure 4b). Averaged over a day, we find an RF of 3.1 W m^{-2} which spans between 0 and 14 W m^{-2}. These estimated RF values are higher than those from Qian et al. (2009) and Hadley et al. (2010) which only considered the effects of BC in snow.

LAP-induced RF increases with elevation, and the peak values occur later at the higher elevations (Figure 4c). The RF is generally smaller than 15 W m^{-2} at low elevations (1,000–2,000 m), with the largest value occurring in late May and disappearing in mid-June as snowpacks disappear. The RF at mid elevations (2,000–3,000 m) peaks in mid-June (30 W m^{-2}) and lasts until the end of the melting season. The RF at high elevations (>3,000 m) has a similar magnitude to mid elevations during March-May and significantly increases in June. Several RF peaks are found in June and July, which can be as high as 60–80 W m^{-2} and correspond well with the snow cover reduction (Figure 4c). As discussed before, the albedo changes between clean and dirty snow generally cause an RF of 10–20 W m^{-2} (Figure 3c). The darkened surface absorbs more sunlight which further accelerates snow melting and causes stronger RF. Snow cover losses from this feedback produce an RF of 80 W m^{-2} at the highest elevations, which is a factor of 2–3 greater than the RF due to instantaneous snow darkening effects.

The LAP-induced RF decreases SWE throughout the melting season (Figure 4d), with the largest reduction (40 mm SWE) in late June. The decrease starts at low elevations (with higher temperatures) and expands to high elevations with later melting season (Figure S4 in Supporting Information S1). The SCF change is small until June and reaches its maximum in earlier July (Figure 4d). Due to LAPs and albedo feedbacks, runoff increases first and decreases in the late melting season. As floods in the Sierra Nevada basins are mainly produced by snowmelt (Huang et al., 2022), the early shift of snowmelt timing is expected to shift snowmelt-driven peak runoff date to earlier by about 5 days.

In the bighorn sheep habitat, LAP-induced RF is generally smaller than 2 W m^{-2} during the accumulation season when deep snow impedes travel and negatively influences the bighorn sheep survival (Conner et al., 2018). Consequently, the impact of LAPs in snow on the bighorn sheep is negligible. In the melting season, LAPs in snow have been shown to decrease SWE and snow depth in June by up to 20 and 70 mm, respectively. The decrease in

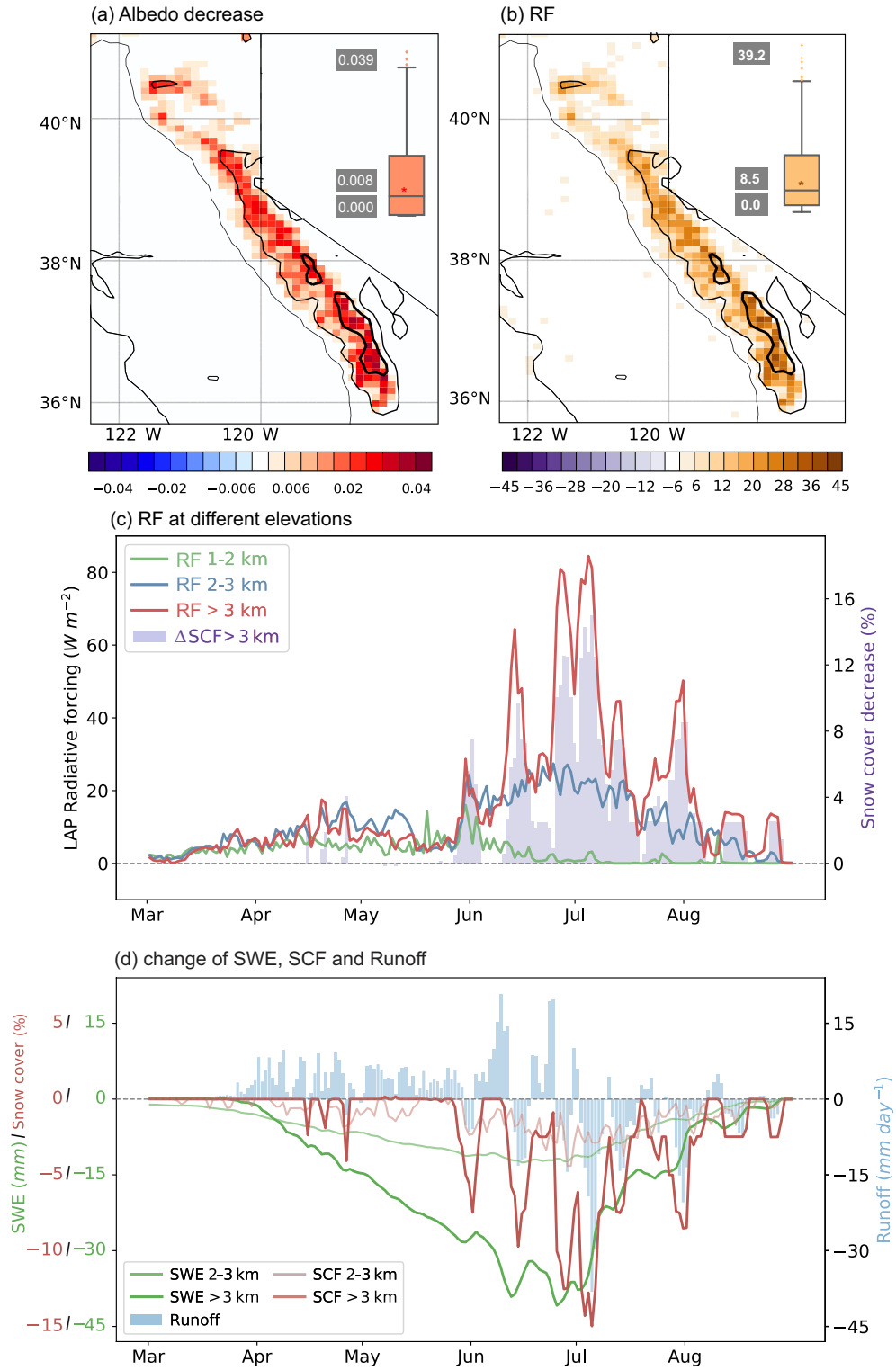

Figure 4. Difference of (a) surface albedo and (b) net shortwave radiation between $WCCS_{aero}$ and $WCCS_{noaero}$ during midday (10:00–14:00 LT) averaged over April–July. The box plots illustrate the distribution of $\Delta\alpha$ (RF) throughout the Sierra Nevada with the mean, maximum, and minimum values labeled on the left; The three contours represent the elevations of 1,000, 2,000, and 3,000 m; (c) RF at different elevations and snow cover fraction change. (d) Change of SWE, SCF, and surface runoff between $WCCS_{aero}$ and $WCCS_{noaero}$.

soil water supply reduces root-zone soil water content by 0.01–0.03 during June-August (Figure S5 in Supporting Information S1), with the largest reduction found in July. The decreasing soil water content tends to reduce forage productivity in early summer (Liu et al., 2019; Liu et al., 2021; Zhang et al., 2019), which deteriorates bighorn sheep diet quality and nutrition status (Stephenson et al., 2020). The nutrition status, typically measured by body mass, is related to the survival and the reproductive success of bighorn sheep (Festa-Bianchet et al., 1997).

4. Conclusions

The LAPs' snow darkening effect has been extensively studied in snow-cover regions, yet the quantification in the Sierra Nevada is rare. This study employs a fully coupled meteorology-chemistry-snow model, WCCS, to investigate the impact of LAPs on snow albedo over the Sierra Nevada (SN). Throughout the SN, WCCS approximately reproduces the observed aerosol spatial patterns and realistically simulates the spatial distribution and temporal evolution of snow cover and SWE. The simulation shows that snow albedo is reduced by 0.013 (0–0.045) during the ablation season due to LAPs in snow, producing a radiative forcing of 4.5 W m^{-2} (0–14.6 W m^{-2}). Despite the lowest AOD in the southeast SN, the largest RF is found there as the higher elevations receive stronger solar irradiance during the ablation period. The model underestimates snow albedo degradation compared to remotely sensed retrievals (0.016 in SPIReS) at the higher elevations, which may be due to uncertainties in snow impurity concentration, insufficient snow aging process, and unrealistically small grain sizes for new snow.

The darkened snow absorbs more sunlight which accelerates melting and exposure of darker surfaces, leading to the well-known "snow albedo feedback." With snow albedo feedbacks, LAPs induce an RF of 8.5 W m^{-2} during the melting season, with the largest RF reaching 80 W m^{-2} in late June. The RF causes a decrease of SWE by 40 mm, shifting the runoff peak earlier.

Data Availability Statement

The PM2.5 and aerosol surface measurements are acquired from U.S. EPA at https://www.epa.gov/outdoor-air-quality-data/download-daily-data and IMPROVE sites at http://vista.cira.colostate.edu/Improve/monitoring-site-browser. SNODAS datasets are from the National Snow & Ice Data Center (NSIDC) at https://nsidc.org/data/g02158; SPIReS dataset is available at https://snow.ucsb.edu/index.php/remotely-sensed-products/. We uploaded the data used in this paper on Zenodo: https://doi.org/10.5281/zenodo.5914858.

Acknowledgments
This research was supported by NASA awards: 80NSSC21K0997, 80NSSC20K1722, 80NSSC20K1349, and 80NSSC18K1489. The Pacific Northwest National Laboratory (PNNL) is operated for DOE by the Battelle Memorial Institute under contract DE-AC05-76RLO1830. We thank Xiaodong Chen, Ying Liu, and Ye Liu from the Pacific Northwest National Laboratory for assistance in model setup and emission generation.

References

Avanzi, F. (2018). *Feather river hydrologic observatory: Improving snowpack forecasting for hydropower generation using intelligent information systems: A report for California's fourth climate change assessment*. California Energy Commission.

Bair, E. H., Rittger, K., Davis, R. E., Painter, T. H., & Dozier, J. (2016). Validating reconstruction of snow water equivalent in California's Sierra Nevada using measurements from the NASA Airborne Snow Observatory. *Water Resources Research*, *52*(11), 8437–8460. https://doi.org/10.1002/2016wr018704

Bair, E. H., Rittger, K., Skiles, S. M., & Dozier, J. (2019). An examination of snow albedo estimates from MODIS and their impact on snow water equivalent reconstruction. *Water Resources Research*, *55*(9), 7826–7842. https://doi.org/10.1029/2019wr024810

Bair, E. H., Stillinger, T., & Dozier, J. (2020). Snow property inversion from remote sensing (SPIReS): A generalized multispectral unmixing approach with examples from MODIS and Landsat 8 OLI. *IEEE Transactions on Geoscience and Remote Sensing*, *59*(9), 7270–7284.

Bair, E. H., Stillinger, T., Rittger, K., & Skiles, S. M. (2021). COVID-19 lockdowns show reduced pollution on snow and ice in the Indus River Basin. *Proceedings of the National Academy of Sciences*, *118*(18).

Barrett, A. P. (2003). *National operational hydrologic remote sensing center snow data assimilation system (SNODAS) products at NSIDC*. National Snow and Ice Data Center, Cooperative Institute for Research in Environmental Sciences.

Buchholz, R., Emmons, L., & Tilmes, S. (2019). CESM2. 1/CAM-chem instantaneous output for boundary conditions. *UCAR/NCAR-Atmospheric chemistry observations and modeling Laboratory*.

Chen, X. D., Duan, Z. R., Leung, L. R., & Wigmosta, M. (2019). A framework to delineate precipitation-runoff regimes: Precipitation versus snowpack in the Western United States. *Geophysical Research Letters*, *46*(22), 13044–13053. https://doi.org/10.1029/2019gl085184

Chen, X. D., Leung, L. R., Wigmosta, M., & Richmond, M. (2019). Impact of atmospheric rivers on surface hydrological processes in Western US watersheds. *Journal of Geophysical Research: Atmospheres*, *124*(16), 8896–8916. https://doi.org/10.1029/2019jd030468

Conner, M. M., Stephenson, T. R., German, D. W., Monteith, K. L., Few, A. P., & Bair, E. H. (2018). Survival analysis: Informing recovery of Sierra Nevada bighorn sheep. *Journal of Wildlife Management*, *82*(7), 1442–1458. https://doi.org/10.1002/jwmg.21490

Creamean, J. M., Suski, K. J., Rosenfeld, D., Cazorla, A., DeMott, P. J., Sullivan, R. C., et al. (2013). Dust and biological aerosols from the Sahara and Asia influence precipitation in the Western US. *Science*, *339*(6127), 1572–1578. https://doi.org/10.1126/science.1227279

Dang, C., Fu, Q., & Warren, S. G. (2016). Effect of snow grain shape on snow albedo. *Journal of the Atmospheric Sciences*, *73*(9), 3573–3583. https://doi.org/10.1175/jas-d-15-0276.1

Doherty, S. J., Warren, S. G., Grenfell, T. C., Clarke, A. D., & Brandt, R. E. (2010). Light-absorbing impurities in Arctic snow. *Atmospheric Chemistry and Physics*, *10*(23), 11647–11680. https://doi.org/10.5194/acp-10-11647-2010

Duniway, M. C., Pfennigwerth, A. A., Fick, S. E., Nauman, T. W., Belnap, J., & Barger, N. N. (2019). Wind erosion and dust from US drylands: A review of `causes, consequences, and solutions in a changing world. *Ecosphere*, *10*(3), e02650. https://doi.org/10.1002/ecs2.2650

Emmons, L. K., Schwantes, R. H., Orlando, J. J., & Geoff, T. (2020). The chemistry mechanism in the community Earth System model version 2 (CESM2). *Journal of Advances in Modeling Earth Systems*, *12*(4), e2019MS001882. https://doi.org/10.1029/2019ms001882

Festa-Bianchet, M., Jorgenson, J. T., Bérubé, C. H., Portier, C., & Wishart, W. D. (1997). Body mass and survival of bighorn sheep. *Canadian Journal of Zoology*, *75*(9), 1372–1379. https://doi.org/10.1139/z97-763

Flanner, M. G., Arnheim, J., Cook, J. M., Dang, C., He, C., Huang, X., et al. (2021). SNICAR-AD v3: A community Tool for modeling spectral snow albedo. *Geoscientific Model Development Discussions*, *2021*, 1–49. https://doi.org/10.5194/gmd-14-7673-2021

Flanner, M. G., & Zender, C. S. (2006). Linking snowpack microphysics and albedo evolution. *Journal of Geophysical Research*, *111*(D12). https://doi.org/10.1029/2005jd006834

Flanner, M. G., Zender, C. S., Hess, P. G., Mahowald, N. M., Painter, T. H., Ramanathan, V., & Rasch, P. J. (2009). Springtime warming and reduced snow cover from carbonaceous particles. *Atmospheric Chemistry and Physics*, *9*(7), 2481–2497. https://doi.org/10.5194/acp-9-2481-2009

Flanner, M. G., Zender, C. S., Randerson, J. T., & Rasch, P. J. (2007). Present-day climate forcing and response from black carbon in snow. *Journal of Geophysical Research*, *112*(D11). https://doi.org/10.1029/2006jd008003

Ginoux, P., Chin, M., Tegen, I., Prospero, J. M., Holben, B., Dubovik, O., & Lin, S. J. (2001). Sources and distributions of dust aerosols simulated with the GOCART model. *Journal of Geophysical Research*, *106*(D17), 20255–20273. https://doi.org/10.1029/2000jd000053

Grell, G. A., & Freitas, S. R. (2014). A scale and aerosol aware stochastic convective parameterization for weather and air quality modeling. *Atmospheric Chemistry and Physics*, *14*(10), 5233–5250. https://doi.org/10.5194/acp-14-5233-2014

Guenther, A., Karl, T., Harley, P., Wiedinmyer, C., Palmer, P. I., & Geron, C. (2006). Estimates of global terrestrial isoprene emissions using MEGAN (model of emissions of gases and aerosols from Nature). *Atmospheric Chemistry and Physics*, *6*(11), 3181–3210. https://doi.org/10.5194/acp-6-3181-2006

Hadley, O. L., Corrigan, C. E., Kirchstetter, T. W., Cliff, S. S., & Ramanathan, V. (2010). Measured black carbon deposition on the Sierra Nevada snow pack and implication for snow pack retreat. *Atmospheric Chemistry and Physics*, *10*(15), 7505–7513.

Hadley, O. L., & Kirchstetter, T. W. (2012). Black-carbon reduction of snow albedo. *Nature Climate Change*, *2*(6), 437–440. https://doi.org/10.1038/nclimate1433

He, C. L., Flanner, M. G., Chen, F., Barlage, M., Liou, K. N., Kang, S. C., et al. (2018). Black carbon-induced snow albedo reduction over the Tibetan plateau: Uncertainties from snow grain shape and aerosol-snow mixing state based on an updated SNICAR model. *Atmospheric Chemistry and Physics*, *18*(15), 11507–11527. https://doi.org/10.5194/acp-18-11507-2018

He, C. L., Liou, K. N., Takano, Y., Chen, F., & Barlage, M. (2019). Enhanced snow absorption and albedo reduction by dust-snow internal mixing: Modeling and parameterization. *Journal of Advances in Modeling Earth Systems*, *11*(11), 3755–3776. https://doi.org/10.1029/2019ms001737

Hersbach, H., Bell, B., Berrisford, P., Hirahara, S., Horányi, A., Muñoz-Sabater, J., et al. (2020). The ERA5 global reanalysis. *Quarterly Journal of the Royal Meteorological Society*, *146*(730), 1999–2049.

He, C. L., Takano, Y., & Liou, K. N. (2017). Close packing effects on clean and dirty snow albedo and associated climatic implications. *Geophysical Research Letters*, *44*(8), 3719–3727. https://doi.org/10.1002/2017gl072916

He, C. L., Takano, Y., Liou, K. N., Yang, P., Li, Q. B., & Chen, F. (2017). Impact of snow grain shape and black carbon-snow internal mixing on snow optical properties: Parameterizations for climate models. *Journal of Climate*, *30*(24), 10019–10036. https://doi.org/10.1175/jcli-d-17-0300.1

Hong, S.-Y., Noh, Y., & Dudhia, J. (2006). A new vertical diffusion package with an explicit treatment of entrainment processes. *Monthly Weather Review*, *134*(9), 2318–2341. https://doi.org/10.1175/mwr3199.1

Huang, H., Fischella, M. R., Liu, Y., Ban, Z., Fayne, J. V., Li, D., et al. (2022). Changes in mechanisms and characteristics of Western U.S. Floods over the last sixty years. *Geophysical Research Letters*, *49*(3), e2021GL097022. https://doi.org/10.1029/2021gl097022

Huang, H., Xue, Y., Li, F., & Liu, Y. (2020). Modeling long-term fire impact on ecosystem characteristics and surface energy using a process-based vegetation–fire model SSiB4/TRIFFID-Fire v1.0. *Geoscientific Model Development*, *13*(12), 6029–6050. https://doi.org/10.5194/gmd-13-6029-2020

Huning, L. S., & AghaKouchak, A. (2018). Mountain snowpack response to different levels of warming. *Proceedings of the National Academy of Sciences USA*, *115*(43), 10932–10937. https://doi.org/10.1073/pnas.1805953115

Iacono, M. J., Delamere, J. S., Mlawer, E. J., Shephard, M. W., Clough, S. A., & Collins, W. D. (2008). Radiative forcing by long-lived greenhouse gases: Calculations with the AER radiative transfer models. *Journal of Geophysical Research*, *113*(D13). https://doi.org/10.1029/2008jd009944

Kang, S. C., Zhang, Y. L., Qian, Y., & Wang, H. L. (2020). A review of black carbon in snow and ice and its impact on the cryosphere. *Earth-Science Reviews*, *210*. https://doi.org/10.1016/j.earscirev.2020.103346

Kapnick, S., & Hall, A. (2010). Observed climate-snowpack relationships in California and their implications for the future. *Journal of Climate*, *23*(13), 3446–3456. https://doi.org/10.1175/2010jcli2903.1

Kirchstetter, T. W., Novakov, T., & Hobbs, P. V. (2004). Evidence that the spectral dependence of light absorption by aerosols is affected by organic carbon. *Journal of Geophysical Research*, *109*(D21).

Lee, W. L., & Liou, K. N. (2012). Effect of absorbing aerosols on snow albedo reduction in the Sierra Nevada. *Atmospheric Environment*, *55*, 425–430. https://doi.org/10.1016/j.atmosenv.2012.03.024

Liu, Y., Guo, W., Huang, H., Ge, J., & Qiu, B. (2021). Estimating global aerodynamic parameters in 1982–2017 using remote-sensing data and a turbulent transfer model. *Remote Sensing of Environment*, *260*, 112428.

Liu, Y., Xue, Y., MacDonald, G., Cox, P., & Zhang, Z. (2019). Global vegetation variability and its response to elevated CO2, global warming, and climate variability – A study using the offline SSiB4/TRIFFID model and satellite data. *Earth System Dynamics.*, *10*(1), 9–29. https://doi.org/10.5194/esd-10-9-2019

Malm, W. C., Sisler, J. F., Huffman, D., Eldred, R. A., & Cahill, T. A. (1994). Spatial and seasonal trends in particle concentration and optical extinction in the United States. *Journal of Geophysical Research*, *99*(D1), 1347–1370. https://doi.org/10.1029/93jd02916

Monteith, K. L., Bleich, V. C., Stephenson, T. R., Pierce, B. M., Conner, M. M., Kie, J. G., & Bowyer, R. T. (2014). Life-history characteristics of mule deer: Effects of nutrition in a variable environment. *Wildlife Monographs*, *186*(1), 1–62. https://doi.org/10.1002/wmon.1011

Morrison, H., Thompson, G., & Tatarskii, V. (2009). Impact of cloud microphysics on the development of trailing stratiform precipitation in a simulated squall line: Comparison of one- and two-moment schemes. *Monthly Weather Review*, *137*(3), 991–1007. https://doi.org/10.1175/2008mwr2556.1

Myhre, G., Shindell, D., Bréon, F.-M., Collins, W., Fuglestvedt, J., Huang, J., et al. (2013). Anthropogenic and natural radiative forcing. *Climate Change*, 423.

Niu, H. W., Kang, S. C., Wang, H. L., Zhang, R. D., Lu, X. X., Qian, Y., et al. (2018). Seasonal variation and light absorption property of carbonaceous aerosol in a typical glacier region of the southeastern Tibetan Plateau. *Atmospheric Chemistry and Physics*, *18*(9), 6441–6460. https://doi.org/10.5194/acp-18-6441-2018

Oaida, C. M., Xue, Y. K., Flanner, M. G., Skiles, S. M., De Sales, F., & Painter, T. H. (2015). Improving snow albedo processes in WRF/SSiB regional climate model to assess impact of dust and black carbon in snow on surface energy balance and hydrology over Western US. *Journal of Geophysical Research: Atmospheres*, *120*(8), 3228–3248. https://doi.org/10.1002/2014jd022444

Oleson, K. W., Lawrence, D. M., Gordon, B., Flanner, M. G., Kluzek, E., Peter, J., et al. (2010). *Technical description of version 4.0 of the community land model (CLM)*.

Painter, T. H., Barrett, A. P., Landry, C. C., Neff, J. C., Cassidy, M. P., Lawrence, C. R., et al. (2007). Impact of disturbed desert soils on duration of mountain snow cover. *Geophysical Research Letters*, *34*(12). https://doi.org/10.1029/2007gl030284

Painter, T. H., Deems, J. S., Belnap, J., Hamlet, A. F., Landry, C. C., & Udall, B. (2010). Response of Colorado River runoff to dust radiative forcing in snow. *Proceedings of the National Academy of Sciences USA*, *107*(40), 17125–17130. https://doi.org/10.1073/pnas.0913139107

Painter, T. H., Dozier, J., Roberts, D. A., Davis, R. E., & Green, R. O. (2003). Retrieval of subpixel snow-covered area and grain size from imaging spectrometer data. *Remote Sensing of Environment*, *85*(1), 64–77. https://doi.org/10.1016/s0034-4257(02)00187-6

Painter, T. H., Duval, B., Thomas, W. H., Mendez, M., Heintzelman, S., & Dozier, J. (2001). Detection and quantification of snow algae with an airborne imaging spectrometer. *Applied and Environmental Microbiology*, *67*(11), 5267–5272. https://doi.org/10.1128/aem.67.11.5267-5272.2001

Painter, T. H., Rittger, K., McKenzie, C., Slaughter, P., Davis, R. E., & Dozier, J. (2009). Retrieval of subpixel snow covered area, grain size, and albedo from MODIS. *Remote Sensing of Environment*, *113*(4), 868–879.

Painter, T. H., Seidel, F. C., Bryant, A. C., Skiles, S. M., & Rittger, K. (2013). Imaging spectroscopy of albedo and radiative forcing by light-absorbing impurities in mountain snow. *Journal of Geophysical Research: Atmospheres*, *118*(17), 9511–9523. https://doi.org/10.1002/jgrd.50520

Qian, Y., Flanner, M. G., Leung, L. R., & Wang, W. (2011). Sensitivity studies on the impacts of Tibetan Plateau snowpack pollution on the Asian hydrological cycle and monsoon climate. *Atmospheric Chemistry and Physics*, *11*(5), 1929–1948. https://doi.org/10.5194/acp-11-1929-2011

Qian, Y., Gustafson, W. I., Leung, L. R., & Ghan, S. J. (2009). Effects of soot-induced snow albedo change on snowpack and hydrological cycle in Western United States based on Weather Research and Forecasting chemistry and regional climate simulations. *Journal of Geophysical Research*, *114*. https://doi.org/10.1029/2008jd011039

Qian, Y., Wang, H. L., Zhang, R. D., Flanner, M. G., & Rasch, P. J. (2014). A sensitivity study on modeling black carbon in snow and its radiative forcing over the Arctic and Northern China. *Environmental Research Letters*, *9*(6). https://doi.org/10.1088/1748-9326/9/6/064001

Qian, Y., Yasunari, T. J., Doherty, S. J., Flanner, M. G., Lau, W. K. M., Ming, J., et al. (2014). Light-absorbing particles in snow and ice: Measurement and modeling of climatic and hydrological impact. *Advances in Atmospheric Sciences*, *32*(1), 64–91. https://doi.org/10.1007/s00376-014-0010-0

Rahimi, S., Liu, X. H., Zhao, C., Lu, Z., & Lebo, Z. J. (2020). Examining the atmospheric radiative and snow-darkening effects of black carbon and dust across the Rocky Mountains of the United States using WRF-Chem. *Atmospheric Chemistry and Physics*, *20*(18), 10911–10935. https://doi.org/10.5194/acp-20-10911-2020

Reheis, M. C. (1997). Dust deposition downwind of Owens (dry) Lake, 1991-1994: Preliminary findings. *Journal of Geophysical Research*, *102*(D22), 25999–26008. https://doi.org/10.1029/97jd01967

Reheis, M. C., & Kihl, R. (1995). Dust deposition in southern Nevada and California, 1984-1989 - relations to climate, source area, and source lithology. *Journal of Geophysical Research*, *100*(D5), 8893–8918. https://doi.org/10.1029/94jd03245

Sarangi, C., Qian, Y., Rittger, K., Bormann, K. J., Liu, Y., Wang, H. L., et al. (2019). Impact of light-absorbing particles on snow albedo darkening and associated radiative forcing over high-mountain Asia: High-resolution WRF-chem modeling and new satellite observations. *Atmospheric Chemistry and Physics*, *19*(10), 7105–7128. https://doi.org/10.5194/acp-19-7105-2019

Sarangi, C., Qian, Y., Rittger, K., Leung, L. R., Chand, D., Bormann, K. J., & Painter, T. H. (2020). Dust dominates high-altitude snow darkening and melt over high-mountain Asia. *Nature Climate Change*, *10*(11), 1045–1051. https://doi.org/10.1038/s41558-020-00909-3

Seidel, F. C., Rittger, K., Skiles, S. M., Molotch, N. P., & Painter, T. H. (2016). Case study of spatial and temporal variability of snow cover, grain size, albedo and radiative forcing in the Sierra Nevada and Rocky Mountain snowpack derived from imaging spectroscopy. *The Cryosphere*, *10*(3), 1229–1244. https://doi.org/10.5194/tc-10-1229-2016

Skiles, S. M., Flanner, M., Cook, J. M., Dumont, M., & Painter, T. H. (2018). Radiative forcing by light-absorbing particles in snow. *Nature Climate Change*, *8*(11), 964–971. https://doi.org/10.1038/s41558-018-0296-5

Skiles, S. M., & Painter, T. (2017). Daily evolution in dust and black carbon content, snow grain size, and snow albedo during snowmelt, Rocky Mountains, Colorado. *Journal of Glaciology*, *63*(237), 118–132. https://doi.org/10.1017/jog.2016.125

Skiles, S. M., & Painter, T. H. (2018). Assessment of radiative forcing by light-absorbing particles in snow from in Situ observations with radiative transfer modeling. *Journal of Hydrometeorology*, *19*(8), 1397–1409.

Stephenson, T. R., German, D. W., Cassirer, E. F., Walsh, D. P., Blum, M. E., Cox, M., et al. (2020). Linking population performance to nutritional condition in an alpine ungulate. *Journal of Mammalogy*, *101*(5), 1244–1256. https://doi.org/10.1093/jmammal/gyaa091

Sterle, K. M., McConnell, J. R., Dozier, J., Edwards, R., & Flanner, M. G. (2013). Retention and radiative forcing of black carbon in eastern Sierra Nevada snow. *The Cryosphere*, *7*(1), 365–374. https://doi.org/10.5194/tc-7-365-2013

Stillinger, T., Roberts, D. A., Collar, N. M., & Dozier, J. (2019). Cloud masking for Landsat 8 and MODIS Terra over snow-covered terrain: Error analysis and spectral similarity between snow and cloud. *Water Resources Research*, *55*(7), 6169–6184. https://doi.org/10.1029/2019wr024932

Thomas, W. H., & Duval, B. (1995). Sierra-Nevada, California, USA, snow algae - snow albedo changes, algal bacterial interrelationships, and ultraviolet-radiation effects. *Arctic and Alpine Research*, *27*(4), 389–399. https://doi.org/10.2307/1552032

US Environmental Protection Agency. (2021). *2017 National Emissions Inventory: January 2021 Updated Release, Technical Support Document Office of Air Quality Planning and Standards*. Air Quality Assessment Division, US Environmental Protection Agency (US EPA).

von Storch, H., Langenberg, H., & Feser, F. (2000). A spectral nudging technique for dynamical downscaling purposes. *Monthly Weather Review*, *128*(10), 3664–3673. https://doi.org/10.1175/1520-0493(2000)128<3664:asntfd>2.0.co;2

Wanders, N., Bachas, A., He, X., Huang, H., Koppa, A., Mekonnen, Z., et al. (2017). Forecasting the hydroclimatic signature of the 2015/16 El Niño event on the Western United States. *Journal of Hydrometeorology*, *18*(1), 177–186. https://doi.org/10.1175/jhm-d-16-0230.1

Wang, T. Y., Jiang, Z., Zhao, B., Gu, Y., Liou, K. N., Kalandiyur, N., et al. (2020). Health co-benefits of achieving sustainable net-zero greenhouse gas emissions in California. *Nature Sustainability*, *3*(8), 597–605.

Warren, S. G., & Wiscombe, W. J. (1980). A model for the spectral albedo of snow. II: Snow containing atmospheric aerosols. *Journal of the Atmospheric Sciences*, *37*(12), 2734–2745. https://doi.org/10.1175/1520-0469(1980)037<2734:amftsa>2.0.co;2

Wiedinmyer, C., Yokelson, R. J., & Gullett, B. K. (2014). Global emissions of trace gases, particulate matter, and hazardous air pollutants from open burning of domestic waste. *Environmental Science & Technology*, *48*(16), 9523–9530. https://doi.org/10.1021/es502250z

Wu, C., Liu, X., Lin, Z., Rahimi-Esfarjani, S., & Lu, Z. (2018). Impacts of absorbing aerosol deposition on snowpack and hydrologic cycle in the Rocky Mountain region based on variable-resolution CESM (VR-CESM) simulations. *Atmospheric Chemistry and Physics*, *18*(2), 511–533. https://doi.org/10.5194/acp-18-511-2018

Wu, L., Gu, Y., Jiang, J., Su, H., Yu, N., Zhao, C., et al. (2018). Impacts of aerosols on seasonal precipitation and snowpack in California based on convection-permitting WRF-Chem simulations. *Atmospheric Chemistry and Physics*, *18*(8), 5529–5547. https://doi.org/10.5194/acp-18-5529-2018

Wu, L., Su, H., Kalashnikova, O., Jiang, J., Zhao, C., Garay, M., et al. (2017). WRF-chem simulation of aerosol seasonal variability in the San Joaquin Valley. *Atmospheric Chemistry and Physics*, *17*(12), 7291–7309. https://doi.org/10.5194/acp-17-7291-2017

Zaveri, R. A., & Peters, L. K. (1999). A new lumped structure photochemical mechanism for large-scale applications. *Journal of Geophysical Research*, *104*(D23), 30387–30415. https://doi.org/10.1029/1999jd900876

Zhang, K., Ali, A., Antonarakis, A., Moghaddam, M., Saatchi, S., Tabatabaeenejad, A., et al. (2019). The sensitivity of north American terrestrial carbon fluxes to spatial and temporal variation in soil moisture: An analysis using radar-derived estimates of root-zone soil moisture. *Journal of Geophysical Research: Biogeosciences*, *124*(11), 3208–3231. https://doi.org/10.1029/2018jg004589

Zhao, C., Hu, Z., Qian, Y., Ruby Leung, L., Huang, J., Huang, M., et al. (2014). Simulating black carbon and dust and their radiative forcing in seasonal snow: A case study over north China with field campaign measurements. *Atmospheric Chemistry and Physics*, *14*(20), 11475–11491. https://doi.org/10.5194/acp-14-11475-2014

Zhao, C., Leung, L. R., Easter, R., Hand, J., & Avise, J. (2013). Characterization of speciated aerosol direct radiative forcing over California. *Journal of Geophysical Research: Atmospheres*, *118*(5), 2372–2388. https://doi.org/10.1029/2012jd018364

References From the Supporting Information

Chapman, E. G., Gustafson, W. I., Easter, R. C., Barnard, J. C., Ghan, S. J., Pekour, M. S., & Fast, J. D. (2009). Coupling aerosol-cloud-radiative processes in the WRF-Chem model: Investigating the radiative impact of elevated point sources. *Atmospheric Chemistry and Physics*, *9*(3), 945–964. https://doi.org/10.5194/acp-9-945-2009

Easter, R. C., Ghan, S. J., Zhang, Y., Saylor, R. D., Chapman, E. G., Laulainen, N. S., et al. (2004). Mirage: Model description and evaluation of aerosols and trace gases. *Journal of Geophysical Research*, *109*(D20). https://doi.org/10.1029/2004jd004571

Fahey, K. M., & Pandis, S. N. (2001). Optimizing model performance: Variable size resolution in cloud chemistry modeling. *Atmospheric Environment*, *35*(26), 4471–4478. https://doi.org/10.1016/s1352-2310(01)00224-2

Kumar, R., Barth, M., Pfister, G., Naja, M., & Brasseur, G. (2014). WRF-chem simulations of a typical pre-monsoon dust storm in northern India: Influences on aerosol optical properties and radiation budget. *Atmospheric Chemistry and Physics*, *14*(5), 2431–2446. https://doi.org/10.5194/acp-14-2431-2014